



Contents lists available at ScienceDirect

Tetrahedron

journal homepage: [www.elsevier.com/locate/tet](http://www.elsevier.com/locate/tet)

## 5,5'-alkylsubstituted indigo for solution-processed optoelectronic devices

Motonori Watanabe<sup>a,\*</sup>, Naoki Uemura<sup>b</sup>, Shintaro Ida<sup>a,c</sup>, Hidehisa Hagiwara<sup>a,c</sup>,  
Kenta Goto<sup>d</sup>, Tatsumi Ishihara<sup>a,b,c,\*</sup>

<sup>a</sup> International Institute for Carbon-Neutral Energy Research (I2CNER), Kyushu University, 744 Motoooka, Nishi-ku, Fukuoka, 819-0395, Japan

<sup>b</sup> Graduated School of Integrated Frontier Science, Department of Automotive Science, Kyushu University, 744 Motoooka, Nishi-ku, Fukuoka, 819-0395, Japan

<sup>c</sup> Department of Applied Chemistry, Kyushu University, 744 Motoooka, Nishi-ku, Fukuoka, 819-0395, Japan

<sup>d</sup> Institute for Materials Chemistry and Engineering, Kyushu University, 744 Motoooka, Nishi-ku, Fukuoka, 819-0395, Japan

### ARTICLE INFO

#### Article history:

Received 14 April 2016

Received in revised form 27 May 2016

Accepted 27 May 2016

Available online xxx

#### Keywords:

Indigo

Substituent effect

Solution process

Precursor method

Photo current

### ABSTRACT

A series of alkylated indigos were synthesized. Alkylated indigos were characterized by NMR, mass spectrometry, absorption spectra, cyclic voltammetry, and density functional theory (DFT) calculations. Propyl and butyl group substituted indigo was most soluble in chloroform and 1,2-dichlorobenzene, and these solubility were 65–89 times increased as compared to the parent indigo. DFT calculations suggested that the presence of the alkyl chains at the 5,5'-position increases the energy of the highest occupied molecular orbital, while reducing the energy of the lowest unoccupied molecular orbital. This theoretical finding was in good agreement with the experimental results. Crystal structures obtained by X-ray diffraction showed one-dimensional  $\pi$ - $\pi$  stacking. Alkylated molecules were converted to leuco structure, and these structures were then converted to the corresponding indigos in the film state. After deposition of the films on TiO<sub>2</sub>/FTO substrate, oxidative photocurrents were observed.

© 2016 Published by Elsevier Ltd.

### 1. Introduction

Indigo and its derivatives are some of the most popular dyes used in pigments and artificial colorants. The crystal structure of Indigo shows a two-dimensional packing orientation due to the presence of intra- and intermolecular hydrogen bond interactions.<sup>1</sup> The former interactions allow a planar structure of the indigo skeleton, giving rise to the  $\pi$  orbital delocalization on the indigo skeleton. The latter interactions lead to the two-dimensional like arrangement of the individual indigo molecules in the crystal structure. Therefore, both intra- and intermolecular interactions contribute to generating the herring-bone-like structure that increases charge transfer, motivating considerable interest in indigos as building blocks and charge-transporting materials.<sup>2–4</sup> Recently, indigos and functionalized indigos were applied for optoelectronic devices, such as field effect transistors,<sup>5–7</sup> solar cells,<sup>8,9</sup> sensors,<sup>10,11</sup> and electrodes for ion batteries.<sup>12,13</sup> In particular, Pitayatanakul et al., reported on the halogen or phenyl group functionalized indigos for organic semiconductors. In this series of compounds, the

indigos showed a herring-bone like structure for the halogen substitution derivatives, whereas a brickwork arrangement of the crystal structure was observed in the case of phenyl-derivatives because of  $\pi$ - $\pi$  interactions arising from the functionalization substitution at 5-position.<sup>14</sup> The iodine derivatives showed good ambipolar properties due to inter-molecular iodine–iodine interactions leading to stronger  $\pi$ - $\pi$  interactions between the indigo skeletons.<sup>15</sup> The group of Troshin reported a similar effect in the indigos substituted by halogens at the 5,5'- and/or 6,6'-positions.<sup>16</sup> These results indicate that in addition to changing the energy difference between the highest occupied and lowest unoccupied molecular orbitals (HOMO and LUMO), the substituted functional group also plays a key role in the charge transport crucial for optoelectronic properties of indigos. The use of an alkyl chain as a substituent is a promising strategy for changing the crystal packing. Furthermore, the presence of alkyl chains can increase the solubility of low-solubility organic materials in organic solvents to enable solution-processed fabrication for optoelectronic applications. This technique is widely applied to solution-processed optoelectronic devices using an organic materials such as tetrathiafulvalene,<sup>17</sup> oligothiophene,<sup>18,19</sup> anthracene,<sup>20</sup> thienoacene,<sup>21</sup> imide,<sup>22</sup> and others.<sup>23</sup> This approach can be used to increase the solubility and change the charge transporting property for

\* Corresponding authors. Tel./fax: +81 92 802 6748; e-mail addresses: [mwata@i2cner.kyushu-u.ac.jp](mailto:mwata@i2cner.kyushu-u.ac.jp) (M. Watanabe), [ishihara@cstf.kyushu-u.ac.jp](mailto:ishihara@cstf.kyushu-u.ac.jp) (T. Ishihara).

<http://dx.doi.org/10.1016/j.tet.2016.05.069>

0040-4020/© 2016 Published by Elsevier Ltd.

indigo. Although Lüttke et al. reported on several types of alkylated 5,5'- and 6,6'-position substituted indigos, a systematic study of these dyes are necessary for understanding the relationships between the series of alkyl chain substitutions and the physical properties of the compounds was not performed.<sup>24</sup> Here we report on the synthesis and physical properties of a series of 5,5'-position alkylated indigos. We also examine the photocurrent response of films fabricated by solution processing from indigos and from leuco-indigos for optoelectronic application (Fig. 1). Moreover, it is found that a suitable chain size can be chosen to change the crystal packing structure to a one-dimensional packing structure, and good charge interaction orientation were demonstrated in the film state. These effects can increase the photocurrent in the spin-coated optoelectronic devices.

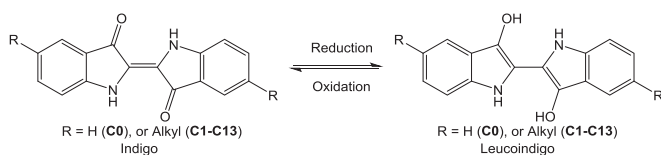


Fig. 1. Interconversion of indigo and leuco-indigo compounds.

## 2. Results and discussion

### 2.1. Synthesis

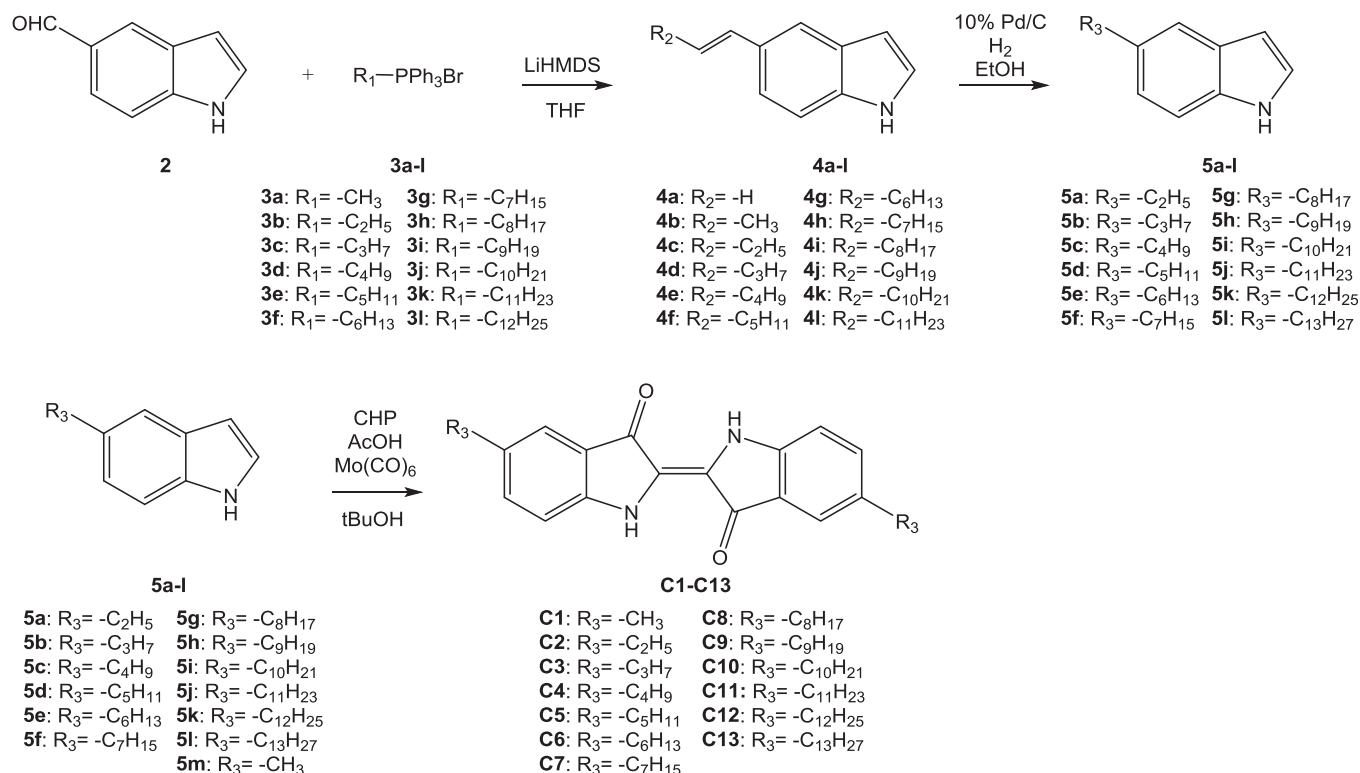
Synthesis of the 5–5' position alkyl chain substituent indigo is illustrated in Scheme 1. Wittig reaction of indole-5-carboxyaldehyde **2** with Wittig salt **3a–3l** gave the alkylene-compounds **4a–4l**, and double bonds were reduced by hydrogen with the Pd/C catalyst to give 5-position alkylated indoles **5a–5l** in good yields. The **5a–5m** were directly coupled using an oxidation

reaction<sup>25</sup> in the presence of Mo(CO)<sub>6</sub> to give the desired indigos **C1–C13**.

### 2.2. Physical properties: absorption spectra, solubility, electrochemical property, and DFT calculations

Absorption spectra of indigo (**C0**) and the alkylated indigos (**C1–C13**) are shown in Fig. 2a. The parent **C0** showed maximum absorption at 600 nm. Relative to **C0**, the absorption peaks of alkylated indigos **C1–C13** were slightly red-shifted to approximately 615–617 nm and showed absorption intensities similar to that of **C0**. Alkyl chains may improve the solubility and/or crystallinity in the solution state. To study the effect of the 5,5'-positioned alkyl chains on the solubility, the solubilities in DCB at 23 °C of **C0–C13** were compared. The saturated amount of indigos at these conditions was estimated using the calibration curve of the absorption spectra. Fig. 2b shows the solubility values obtained for these dyes. The solubility of the parent indigo molecule was reported as 0.038 mmol/L (ca. 10 mg/L) in chloroform.<sup>26</sup> We found that the solubility of **C0** in chloroform at 23 °C is 0.053 mmol/L, and in DCB at 23 °C is 0.012 mmol/L. In contrast, in the same conditions, alkylated dyes **C1–C13** showed solubilities in the 0.056–4.73 mmol/L range for chloroform, and in the 0.006–0.78 mmol/L range in DCB. As seen in Fig. 2a and Fig. S9, the propyl (**C3**) and butyl chain (**C4**) substituted indigos showed particularly high solubility values. The hydrophobicity of alkyl chains assists the solvation of a series of  $\pi$ -conjugated organic molecules in an organic solvent.<sup>23</sup> Our work shows that the **C1–C13** series of compounds also displays this effect of alkyl chain hydrophobicity on solvation.

To understand the electronic properties of **C1–C13**, cyclic voltammetry (CV) measurements were performed. Due to the low solubility of all of the synthesized compounds except for **C3** and **C4** at 23 °C, CV measurements for all compounds were conducted at



Scheme 1. Synthetic route to obtain alkylated indigos **C1–C13**.

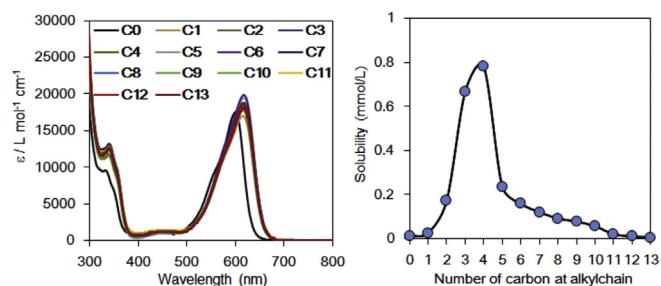


**Fig. 2.** Absorption spectra of synthesized alkylated indigos (left) and their solubilities in 1,2-dichlorobenzene at 23 °C (right).

140 °C in DCB solutions. Fig. 3 shows the cyclic voltammograms for selected compounds. In these conditions, all compounds showed quasi-stable reduction curves and unstable oxidation curves (Fig. S1). The reduction potentials obtained for **C1–C13** varied between  $-0.79$  to  $-0.85$  V (vs NHE) with these values similar to the  $-0.80$  V (vs NHE) value for **C0**. Based on the onset potentials ( $E_{0-0}$ ) of 1.96 eV for **C0** and 1.88 eV for the **C1–C13** obtained from the absorption spectra and the negative shift of LUMO energies observed in cyclic voltammetry, the oxidation potentials for **C0** and **C1–C13** were estimated as +1.15 V (vs NHE) and +1.09 to +1.03 V (vs NHE), respectively. This suggests that the alkylation on the 5,5'-positions slightly reduces the electron accepting properties and increases the electron donating abilities. The reduction of electron affinity saturated for the octyl group in the **C8** (Table S1).

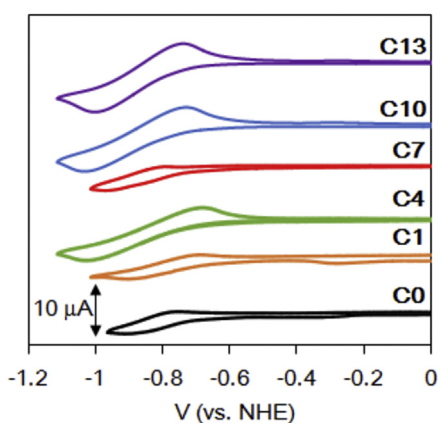


**Fig. 3.** Cyclic voltammogram of selected indigos in 1,2-dichlorobenzene with 0.1 M Tetrabutylammonium tetrafluoroborate solution at 140 °C.

The physical properties of the compounds **C0–C13** were further verified by density functional theory (DFT, B3LYP/6-31Gd) calculations. Fig. 4 shows the HOMOs and LUMOs of selected compounds. For all molecules, HOMOs and LUMOs were delocalized over the indigo skeleton, suggesting that the absorption bands at 600 nm for parent indigo and at 615–617 nm for alkylated indigos are of the  $\pi-\pi^*$  transition type (Fig. S2). Examination of the absorption spectra and cyclic voltammetry results shows that HOMO and/or LUMO energy levels are decreased by the introduction of alkyl chains. Comparison of DFT calculation results for the parent **C0** and alkylated indigos **C1–C13** shows that the presence of alkyl chains at the 5,5'-position decreases both the HOMO and LUMO energies. Furthermore, cyclic voltammetry measurements for alkylated indigos **C1–C13** showed a gradual decrease of electron affinities with increasing length of the alkyl chain that saturates at **C5**. The DFT HOMO–LUMO energy gaps for **C1–C13** were 2.45 eV,

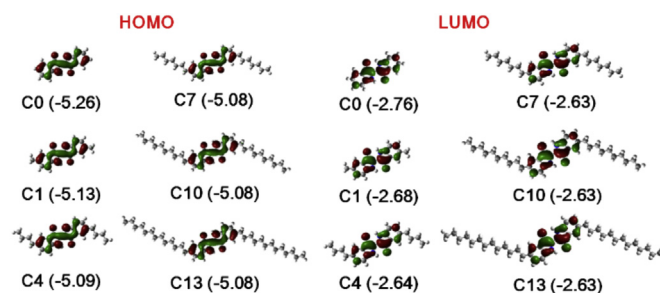


**Fig. 4.** HOMO and LUMO orbitals of indigos. Energy potentials (eV) are given in parenthesis.

supporting the same energy gap values for **C1–C13** and the lowest energy peaks obtained by experimental results. Although there were some differences between the DFT results and the experimental results such as the saturation of the HOMO–LUMO energy difference at a higher alkyl chain length, the overall trends found by DFT calculations were in good agreement with the experimental results. The absorption energy, cyclic voltammetry, and DFT results are summarized in Table S1.

### 2.3. X-ray crystallographic study

The crystal structure of the parent indigo compound was reported by Krautscheid et al.<sup>1</sup> The structure showed a  $\pi-\pi$  stacking at the distance of 3.41 Å along the b-axis with 2.168 Å N–H $\cdots$ O inter-molecular hydrogen bond interaction along the c-axis, demonstrating the two dimensional array crystal packing.

As described below, the **C7** alkylated indigo shows the highest photoresponse in film form. When the solution of the **C7** in 1,2-dichlorobenzene was slowly evaporated, platelet blue coloured crystals were obtained. The **C7** structure has all-trans conformation of alkyl chains (Fig. 5a).

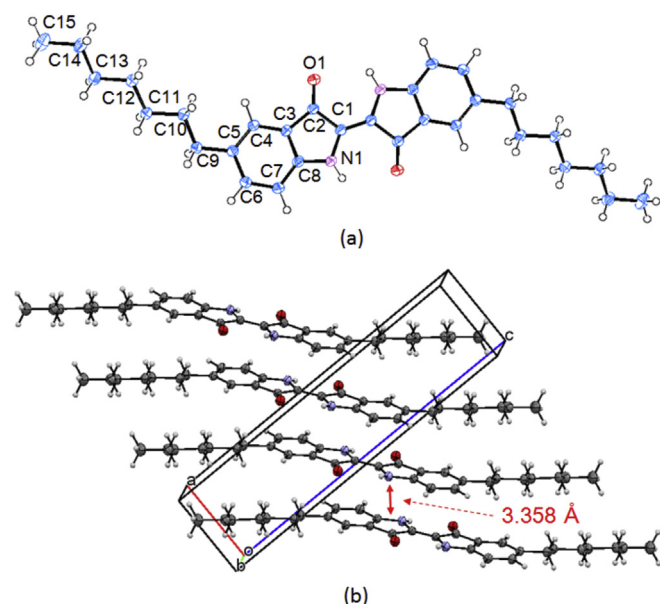


**Fig. 5.** X-ray crystallographic analysis results for **C7**.

These extended alkyl chains allow one dimensional packing of indigo moieties. The indigo skeleton was  $\pi-\pi$  stacked at the distance of 3.358 Å. Furthermore, intermolecular hydrogen bonding at N–H $\cdots$ O (2.361 Å) was found along the b-axis and the alkyl chains

were elongated on the c-axis. This one dimensional packing structure is different from the 2D interactions found in the structure of the parent indigo compound. The one-dimensional stacking moiety is dominated by the interdigitation of the alkyl chain with the van der Waals interaction as the driving force (Fig. 5b).<sup>23</sup> We also successively analysed the single crystal of **C8**. This crystal packing structure showed similar structure with the **C7** (Fig. S3).

#### 2.4. Interconversion of indigos to corresponding leuco-indigos: film state properties, and photocurrent measurements

In addition to increasing the solubility in organic solvents, we found that alkylation also affected the optoelectronic properties because the hydrophobic interaction of alkyl chains between the molecules will affect charge transport. Therefore, solution-processed indigo-coated substrates were fabricated for the measurement of the photoelectrochemical properties to elucidate the effect of indigo alkylation in the solid state. To increase the indigo solubility and enable the use of solution processing, we also investigated the corresponding leuco-indigos in a EtOH solution.

Fig. 6a showed the typical conversion results of **C0** and **C4** with NaOH and Na<sub>2</sub>S<sub>2</sub>O<sub>4</sub> in ethanol solution. When the indigo of ethanol solution was added to NaOH and Na<sub>2</sub>S<sub>2</sub>O<sub>4</sub> with heating in Ar atmosphere, the blue colour indigos disappeared, changing to a pale yellow colour. In the absorption spectra, the characteristic indigo peaks at around 600 nm disappeared for both leuco-**C0** (**LC0**) and leuco-**C4** (**LC4**). Both solutions showed similar structures, suggesting that alkylated indigos can also convert leuco structures. These reaction solutions were drop-cast on a glass substrate under Ar atmosphere with the obtained films shown in Fig. 6b. The films showed no characteristic peaks and strong absorption intensities due to the influence of sodium salts. Conversely, after exposure to air with washing by water to remove the sodium salts, the substrates showed characteristic new peaks at around 670 nm for converted-**C0** (**C0<sub>L</sub>**) and 613 nm for converted-**C4** (**C4<sub>L</sub>**). This suggested that the leuco-indigos were oxidised and converted to the corresponding indigos under air (oxygen), indicating that alkylated leuco-indigos could be converted to their corresponding indigos under air in the film state. These peaks were shifted as compared to the peak of the solutions.

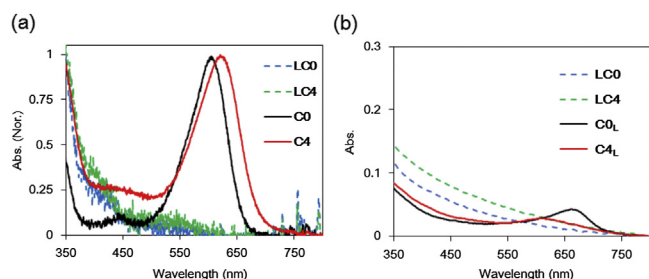


Fig. 6. Absorption spectra (a) before treatment of indigos (**C0** and **C4**) and after treatment with NaOH and Na<sub>2</sub>S<sub>2</sub>O<sub>4</sub> (**LC0** and **LC4**) in EtOH. (b) spin-coated films on glass substrates of leuco-indigos under Ar atmosphere (**LC0** and **LC4**) and after exposure to air (**C0<sub>L</sub>** and **C4<sub>L</sub>**).

When **C0** and **C4** of solution were drop cast to a glass substrate directly, the peak of **C0** and **C4** were red shifted due to aggregate structures were formed such as J-aggregation (Fig. S4). Comparing the results of drop-casted indigo films and the films produced from leuco-indigos, the film of **C0<sub>L</sub>** from **LC0** on glass may has an aggregation state such as J-aggregation, while **C4<sub>L</sub>** from **LC4** has amorphous-like or H-aggregation state because the film **C4<sub>L</sub>** of peak was similar peak in that of solution state.

We expected that a photocurrent will be enhanced by the strongly increased solubility due to the alkyl chain effect as found for the **C4** compound. We first tried to spin-coat these compounds on a fluorine-doped tin oxide (FTO) substrate; however, the coating did not remain on the film in our fabrication conditions. Therefore, we used a TiO<sub>2</sub> film-coated FTO substrate to increase the adhesion of the film by taking advantage of the higher roughness of the TiO<sub>2</sub> film. To remove the photoresponse due to the TiO<sub>2</sub> film, we used a band-pass filter to filter out irradiation at wavelengths smaller than 495 nm. Fig. 7a shows the photocurrent profiles of the **C4**-coated TiO<sub>2</sub> films. The bare substrate (TiO<sub>2</sub> film) did not show a photocurrent response. Conversely, in the case of the spin-coated **C4** (saturated in CHCl<sub>3</sub>, 1200 rpm, 60 s), we observed the increase of positive photocurrent. The spin-coated film of **C4<sub>L</sub>** (From 40 mM **LC4** in EtOH, 1200 rpm, 60s) showed a much stronger response than **C4**.

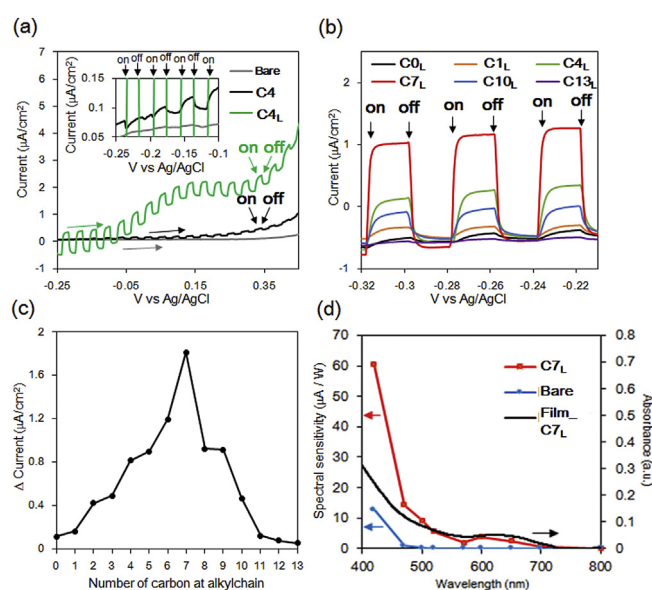


Fig. 7. Photocurrent profiles of indigo dyes on TiO<sub>2</sub> film/FTO substrate. (a) Chopped profile of **C4** coated TiO<sub>2</sub> film on FTO. Inset: enlarged profiles at  $-0.25$  to  $-0.1$  V. **C4** is directly coated by **C4** solution (saturated in CHCl<sub>3</sub>). **C4<sub>L</sub>** is coated by leuco-indigo precursor **LC4** and then converted to **C4** by exposure to air. (b) and (c): Photocurrent response of selected alkylated indigos from leuco-indigo precursors, and photocurrent density dependence profiles of indigos between  $-0.28$  and  $-0.27$  V. (d) Spectral sensitivity at 0 V (vs Ag/AgCl). 0.1 M Na<sub>2</sub>SO<sub>4</sub>, 50 mM TEOA aqueous solution (pH=10). 300-W Xe lamp was used. Red: **C7<sub>L</sub>** (from **C7** precursor) on TiO<sub>2</sub> film/FTO substrate. Blue: TiO<sub>2</sub> film/FTO substrate. Black: Absorption spectra of **C7<sub>L</sub>** on TiO<sub>2</sub> film/FTO substrate.

The absorption bands of **C4** and **C4<sub>L</sub>** on TiO<sub>2</sub>/FTO are shown in Fig. S5. We found the similar absorption peaks of both film at ca. 615 nm, while absorption intensity of **C4<sub>L</sub>** was higher than **C4**, suggesting that the leuco-based film showed much better adhesion on the TiO<sub>2</sub> film due to the higher solubility and increased compound concentration in solution. However, the low solubility of **C4** gives rise to poor results for the coating on the TiO<sub>2</sub>/FTO film, and the obtained photocurrent response is therefore very weak.

We then systematically investigated the effect of alkyl chain length on the photocurrent for the leuco-precursor compounds. We found that the photocurrent magnitude increased when the carbon number of the alkyl chain was increased up to 7 (**C0<sub>L</sub>** to **C7<sub>L</sub>**) and then decreased for carbon numbers from 7 to 13 (**C7<sub>L</sub>** to **C13<sub>L</sub>**, Fig. 7b, c and Fig. S6). The dependence of the photocurrent on the irradiation wavelength was measured for the **C7<sub>L</sub>**-film that showed the highest response (Fig. 7d). Although for wavelengths lower

than 500 nm, the observed spectral sensitivity included the component due to the light response from TiO<sub>2</sub> and FTO, the C<sub>7</sub><sub>L</sub>-film showed the spectral sensitivity corresponding to the original absorption spectra of C<sub>7</sub><sub>L</sub> for wavelengths higher than 500 nm.

The differences in the photocurrent results were somewhat different from the trends in the solubility of the corresponding alkylated indigos. X-ray diffraction (XRD) patterns of the substrates showed same peaks with similar intensities for anatase and FTO, and no peaks corresponding to indigo structure were found (Fig. 8 and Fig. S7). This result indicates that all of indigo compounds are in a poorly-crystalline or amorphous state. Therefore, the effect of crystallinity for the difference of magnitudes of current density can be neglected.

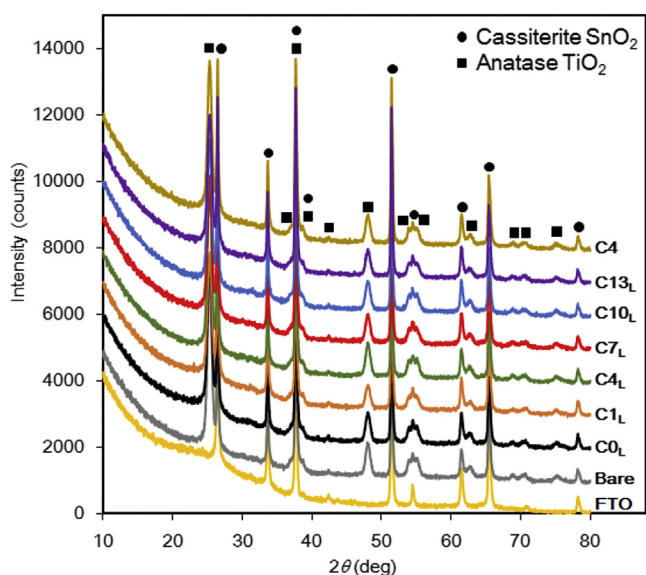


Fig. 8. XRD patterning of indigo-coated TiO<sub>2</sub> film on FTO substrate. Bare: TiO<sub>2</sub> film on FTO.

The absorption bands of indigo compounds on TiO<sub>2</sub>/FTO are shown in Fig. 9 and Fig. S8. The peaks of the lowest energy bands in the indigo absorption spectra first showed a red-shift from C<sub>0</sub><sub>L</sub> to C<sub>7</sub><sub>L</sub>, followed by a blue-shift from C<sub>7</sub><sub>L</sub> to C<sub>13</sub><sub>L</sub>. For C<sub>0</sub><sub>L</sub> on glass substrate, the absorption peak was observed at 670 nm, the peak for C<sub>0</sub><sub>L</sub> on TiO<sub>2</sub>-FTO films was much broader and was blue-shifted to around 582 nm, suggesting a disordered structure. Conversely, the comparison of the peaks from C<sub>1</sub><sub>L</sub> to C<sub>7</sub><sub>L</sub> showed that the peaks became more well-defined and showed an absorption band at 623 nm for C<sub>7</sub><sub>L</sub>. Although this C<sub>7</sub><sub>L</sub> peak is also blue shifted from the

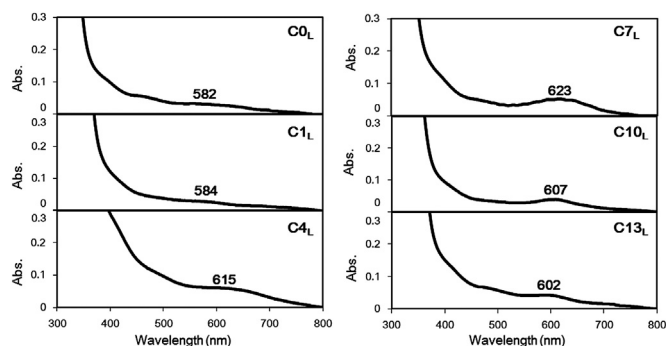


Fig. 9. Absorption spectra of indigo-coated TiO<sub>2</sub> films on FTO substrates.

original peak on the glass substrate, the well-defined peak shape suggested a more ordered orientation on the TiO<sub>2</sub> film. Therefore, the C<sub>7</sub><sub>L</sub>-coated TiO<sub>2</sub>/FTO film showed a good photo current. Conversely, from C<sub>7</sub><sub>L</sub> to C<sub>13</sub><sub>L</sub>, the lowest energy peaks again became broadened and blue-shifted to around 602 nm, indicating increased disorder on the TiO<sub>2</sub> film and leading to small photocurrent values.

The mechanism of the observed photocurrent measurement is proposed in Fig. 10. The energy of the conduction bands (CB) of TiO<sub>2</sub> is -0.5 eV (vs NHE), and the LUMO and HOMO energy levels of the indigos were estimated to be approximately from -0.79 to -0.85 to +1.15 to +1.03, respectively. The energy level of TEOA is +0.80 eV. Based on these energies, the injection of electrons to the CB of TiO<sub>2</sub> from indigos in the excited state is the reasonable electron pathway. Thus, oxidative photocurrent was observed during photoirradiation.

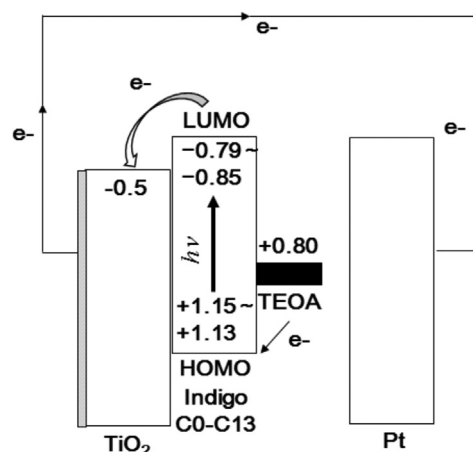


Fig. 10. Schematic energy diagram and energy flow.

### 3. Summary

A series of alkylated indigos were synthesized from 5-alkylated indoles in the presence of Mo(CO)<sub>6</sub>. These compounds showed similar physical properties in absorption spectra and cyclic voltammetry measurements. The solubility in halogen organic solvents such as 1,2-dichlorobenzene was increased when the butyl group was introduced on the 5,5'-position, with further increases obtained when longer alkyl chain were attached. X-ray diffraction showed that the C<sub>7</sub> compound exhibits one dimensional  $\pi$ - $\pi$  stacking array along the *a*-axis. Alkylated molecules were converted to leuco structures, and these structures were then converted to their corresponding indigos in the film state. Upon deposition on the TiO<sub>2</sub>/FTO substrate, the films showed oxidative photocurrents. The alkyl chains were shown to affect the magnitude of ordering of orientation on the TiO<sub>2</sub>/FTO substrate. C<sub>7</sub> showed the most ordered absorption spectra; therefore, the strongest photocurrent was achieved for this compound. Studies of other photoelectronic devices based on the molecules were explored in this work or the studies of their modified structures are ongoing.

## 4. Experimental section

### 4.1. General information

<sup>1</sup>H and <sup>13</sup>C NMR spectra were recorded on Bruker (ascend 400/ascend 600 MHz) spectrometer in CDCl<sub>3</sub>. Chemical shifts are

reported in  $\delta$  scale downfield from the peak for tetramethylsilane. Absorption spectra were recorded on a Shimadzu UV-3600 spectrophotometer and Hamamatsu photonics PMA-11. The redox potentials were measured by using cyclic voltammetry on BAS ALS1200B. All measurements were carried out in 1,2-dichlorobenzene (DCB) solutions containing 0.1 M tetrabutylammonium hexafluorophosphate (TBAPF<sub>6</sub>) as supporting electrolyte at ambient condition after purging with Ar. The conventional three electrode configuration was employed, which consists of a glassy carbon working electrode, a platinum counter electrode, and a Ag/Ag<sup>+</sup> reference electrode calibrated with ferrocene/ferrocenium (Fc/Fc<sup>+</sup>) as an external reference. Mass spectra were recorded on a JEOL JMS-700 MStation double focusing mass spectrometer. XRD pattern of **C0–C13**/TiO<sub>2</sub>/FTO substrates were measured with Rigaku SmartLab. Chromatographic separations were carried out by using silica gel from Kanto Kieselgel si 60 (40–63  $\mu$ m). 5-methylindole (**5m**) was purchased from Sigma–Aldrich, which was used without further purification.

#### 4.2. Conversion of indigos to leuco-indigos

For spin-coated thin-film on TiO<sub>2</sub>/FTO substrate or glass substrate, 0.04 mmol of indigo, 160 mg (4 mmol) of NaOH, 35 mg (0.2 mmol) of Na<sub>2</sub>S<sub>2</sub>O<sub>4</sub> was added in ethanol (1 mL) under Ar atmosphere, and it was heated 70 °C until the suspended indigo was solved and solution colour was turned from blue to pale yellow. After conversion from leuco-indigos to indigos, it was used for fabrication without further purifications. The conversion was confirmed by absorption spectra.

#### 4.3. Fabrication of indigo-coated TiO<sub>2</sub>/FTO substrate

The FTO conducting glass (FTO glass, fluorine doped tin oxide over-layer, transmission >90% in the visible, sheet resistance 7  $\Omega$  square<sup>-1</sup>), titania-oxide pastes of Ti-Nanoxide T/SP was purchased from Solaronix. A thin film of TiO<sub>2</sub> (8  $\mu$ m) was coated on a FTO glass substrate. The CHCl<sub>3</sub> solution of indigos were spin-coated (1200 rpm, 60s) on the TiO<sub>2</sub>/FTO substrate through membrane filter in grove box (MBRAUN MB150B-G, >1 ppm O<sub>2</sub> and H<sub>2</sub>O). The precursor methods, leuco-indigos that were also prepared in the glove box, were fabricated as same manner with CHCl<sub>3</sub> solution. After spin-coated of leuco-indigo on substrates, there were exposed on air (O<sub>2</sub>) to convert indigo and washed with DI water to remove sodium salt. The active area was controlled at a dimension of 1.5 cm<sup>2</sup>.

#### 4.4. Photocurrent measurement

Photocurrent was measured on BAS ALS1200B. All measurements were carried out in DI-water solutions containing 0.1 M Na<sub>2</sub>SO<sub>4</sub> as supporting electrolyte and 50 mM triethanol amine for electron donor. The aqueous solution showed 10 pH. Measurements were accomplished at ambient condition. The conventional three electrode configuration was employed, which consists of indigo-coated TiO<sub>2</sub> film/FTO substrate as working electrode, a platinum mesh as counter electrode, and Ag/AgCl as reference electrode.

The photo-current properties were obtained under a 300 W Xe lamp (ASAHI SPECTRA, MAX-303), and passed through a long-pass filter (Edmund optics, >495 nm cut off). The spectra sensitivity was measured with band-pass filter (ASAHI SPECTRA) and further calibrated using a reference Si-photo diode (Hamamatsu photonics K. K., S1337-1010BQ).

#### 4.5. X-ray crystallographic study

Single crystals of the **C7** and **C8** form suitable for X-ray analysis were obtained by recrystallization from DCB. The X-ray data were collected on a Rigaku Saturn724 diffractometer using multi-layer mirror monochromatic Mo K $\alpha$  radiation ( $\lambda=0.71075$  Å). The structural determination was performed using the direct method technique with SIR 2011. All calculations were performed using the CrystalStructure crystallographic software package except for refinement, which was performed using SHELXL2013. All-non-hydrogen atoms were refined with anisotropically. Crystallographic data for the structural analyses of **C7** and **C8** have been deposited to the Cambridge Crystallographic Data Centre (CCDC) as 1469332 and 1469331, respectively.

#### 4.6. Theoretical computations

Geometry optimization of **C0–C13** were carried out by the DFT method at the B3LYP/6-31G(d) level using Gaussian09 Rev. C.01 suite of programs. The frequency analyses were carried out for the optimized structures to give no imaginary frequency.

#### 4.7. Synthesis of dyes

**4.7.1. 5-Ethyl-1H-indole (5a).** To a three-necked flask containing a mixture of methyltriphenylphosphonium bromide (2.58 g, 7.23 mmol) and THF was dropwise hexamethyldisilazane lithium salt (7.23 mmol, 1.6 M in THF) at –10 °C. After soluble of methyltriphenylphosphonium bromide, the mixture was dropwise indole-5-carboxyaldehyde (700 mg, 4.83 mmol) in THF (10 mL) at –78 °C over 30 min. The reaction mixture was stirred at –78 °C for additional 1 h, then allowed to stirring at room temperature overnight. The mixture was quenched with satd NH<sub>4</sub>Cl (aq), then extracted with ethyl acetate. The organic phase was combined and washed with brine, and dried over anhydrous MgSO<sub>4</sub>. Evaporation of the solvent gave a crude product, which was purified by silica gel chromatograph by EA:hexane (1:5) as eluent. The pale yellow liquid was isolated product of 5-vinyl-1H-indole **4a** (459 mg), which was used next reaction without further purification. The mixture of **4a**, ethanol (10 mL), and 10%Pd/C (46 mg, 10wt % of vinyl indole) was bubbled 10 min with hydrogen gas, then the mixture was stirred at room temperature under hydrogen atmosphere (760 Torr) for 12 h. After reaction, Pd/C was removed by filtration through Celite, then evaporated of solvent to dryness. The product was purified by silica gel column chromatograph by EA:hexane (1:5) as eluent. Pale-yellow oil of **5a** was obtained in 35% yield (in two steps, 242 mg, 1.67 mmol).  $\delta_{\text{H}}$  (400 MHz, CDCl<sub>3</sub>) 8.05 (br s, 1H), 7.46 (s, 1H), 7.31 (d, 1H,  $J=8.3$  Hz), 7.17 (t, 1H,  $J=2.8$  Hz), 7.06 (dd, 1H,  $J=8.3, 1.4$  Hz), 6.51–6.48 (m, 1H), 2.74, (dd, 2H,  $J=15.2, 7.6$  Hz), 1.28 (t, 3H,  $J=7.6$  Hz),  $\delta_{\text{C}}$  (100 MHz, CDCl<sub>3</sub>) 135.8, 134.2, 128.1, 124.2, 122.6, 119.1, 110.7, 102.3, 29.0, 16.5.

Compound **5b–I** were synthesized according to the similar procedure as that of **5a**.

**4.7.2. 5-Propyl-1H-indole (5b).** Pale yellow oil. 65% yield.  $\delta_{\text{H}}$  (400 MHz, CDCl<sub>3</sub>) 8.06 (br s, 1H), 7.44 (s, 1H), 7.32 (d, 1H,  $J=8.3$  Hz), 7.17 (t, 1H,  $J=2.8$  Hz), 7.03 (dd, 1H,  $J=8.3, 1.4$  Hz), 6.49 (t, 1H,  $J=2.0$  Hz), 2.67, (t, 2H,  $J=7.4$  Hz), 1.73–1.63 (m, 2H), 0.97 (t, 3H,  $J=3.4$ )  $\delta_{\text{C}}$  (100 MHz, CDCl<sub>3</sub>) 134.3, 134.1, 128.0, 124.1, 123.1, 119.9, 110.6, 102.3, 38.2, 25.3, 13.9.

**4.7.3. 5-Butyl-1H-indole (5c).** Pale yellow oil. 69% yield.  $\delta_{\text{H}}$  (400 MHz, CDCl<sub>3</sub>) 8.06 (br s, 1H), 7.44 (s, 1H), 7.31 (d, 1H,  $J=8.3$  Hz), 7.17 (t, 1H,  $J=2.8$  Hz), 7.04 (dd, 1H,  $J=8.3, 1.4$  Hz), 6.49 (t, 1H,  $J=2.1$  Hz), 2.70 (t, 2H,  $J=7.6$  Hz), 1.68–1.60 (m, 2H), 1.42–1.33 (m,

2H), 0.93 (t, 3H,  $J=7.3$ )  $\delta_C$  (100 MHz,  $CDCl_3$ ) 134.3, 134.2, 128.0, 124.2, 123.1, 119.8, 110.6, 102.2, 35.7, 34.5, 22.4, 14.0.

**4.7.4. 5-Pentyl-1H-indole (5d).** Pale yellow oil. 66% yield.  $\delta_H$  (400 MHz,  $CDCl_3$ ) 8.06 (br s, 1H), 7.44 (s, 1H), 7.31 (d, 1H,  $J=8.3$  Hz), 7.18 (t, 1H,  $J=2.8$  Hz), 7.04 (dd, 1H,  $J=8.3, 1.4$  Hz), 6.49 (t, 1H,  $J=2.1$  Hz), 2.69 (t, 2H,  $J=7.6$  Hz), 1.70–1.62 (m, 2H), 1.36–1.31 (m, 4H), 0.89 (t, 3H,  $J=6.9$ )  $\delta_C$  (100 MHz,  $CDCl_3$ ) 134.4, 134.3, 128.0, 124.1, 123.1, 119.8, 110.6, 102.3, 36.0, 32.0, 31.6, 22.6, 14.1.

**4.7.5. 5-Hexyl-1H-indole (5e).** Pale yellow oil. 65% yield.  $\delta_H$  (400 MHz,  $CDCl_3$ ) 8.04 (br s, 1H), 7.44 (s, 1H), 7.30 (d, 1H,  $J=8.3$  Hz), 7.17 (t, 1H,  $J=2.8$  Hz), 7.03 (dd, 1H,  $J=8.3, 1.6$  Hz), 6.49–6.47 (m, 1H), 2.69 (t, 2H,  $J=7.8$  Hz), 1.69–1.61 (m, 2H), 1.40–1.25 (m, 6H), 0.88 (t, 3H,  $J=7.0$ )  $\delta_C$  (100 MHz,  $CDCl_3$ ) 134.4, 134.3, 128.0, 124.2, 123.1, 119.8, 110.6, 102.3, 36.1, 32.3, 31.8, 29.1, 22.7, 14.1.

**4.7.6. 5-Heptyl-1H-indole (5f).** Pale yellow oil. 73% yield.  $\delta_H$  (600 MHz,  $CDCl_3$ ) 8.03 (br s, 1H), 7.43 (s, 1H), 7.29 (d, 1H,  $J=8.3$  Hz), 7.16 (t, 1H,  $J=2.9$  Hz), 7.03 (dd, 1H,  $J=8.3, 1.4$  Hz), 6.49–6.47 (m, 1H), 2.69 (t, 2H,  $J=7.7$  Hz), 1.69–1.61 (m, 2H), 1.39–1.22 (m, 8H), 0.88 (t, 3H,  $J=6.8$ )  $\delta_C$  (125 MHz,  $CDCl_3$ ) 134.4, 134.3, 128.1, 124.3, 123.1, 119.8, 110.7, 102.2, 36.2, 32.4, 32.0, 29.5, 29.4, 22.8, 14.2.

**4.7.7. 5-Octyl-1H-indole (5g).** Pale yellow oil. 53% yield.  $\delta_H$  (400 MHz,  $CDCl_3$ ) 8.06 (br s, 1H), 7.43 (s, 1H), 7.30 (d, 1H,  $J=8.3$  Hz), 7.17 (t, 1H,  $J=2.8$  Hz), 7.03 (dd, 1H,  $J=8.3, 1.5$  Hz), 6.50–6.47 (m, 1H), 2.69 (t, 2H,  $J=7.6$  Hz), 1.69–1.60 (m, 2H), 1.40–1.21 (m, 10H), 0.88 (t, 3H,  $J=7.0$ )  $\delta_C$  (100 MHz,  $CDCl_3$ ) 134.4, 134.3, 128.1, 124.1, 123.1, 119.8, 110.6, 102.3, 36.1, 32.3, 31.9, 29.6, 29.4, 29.3, 22.7, 14.1.

**4.7.8. 5-Nonyl-1H-indole (5h).** Pale yellow solid. 48% yield. Mp: 41–42 °C.  $\delta_H$  (400 MHz,  $CDCl_3$ ) 8.02 (br s, 1H), 7.43 (s, 1H), 7.29 (d, 1H,  $J=8.3$  Hz), 7.16 (t, 1H,  $J=2.5$  Hz), 7.03 (d, 1H,  $J=8.3$  Hz), 6.48 (s, 1H), 2.69 (t, 2H,  $J=7.6$  Hz), 1.69–1.60 (m, 2H), 1.40–1.20 (m, 12H), 0.87 (t, 3H,  $J=7.9$ )  $\delta_C$  (100 MHz,  $CDCl_3$ ) 134.41, 134.4, 128.1, 124.1, 123.1, 119.8, 110.6, 102.3, 36.1, 32.3, 31.9, 29.6, 29.4, 29.3, 22.7, 14.1.

**4.7.9. 5-Decyl-1H-indole (5i).** Pale yellow solid. 89% yield. Mp: 298–299 °C.  $\delta_H$  (400 MHz,  $CDCl_3$ ) 8.03 (br s, 1H), 7.43 (s, 1H), 7.30 (d, 1H,  $J=8.2$  Hz), 7.16 (s, 1H), 7.03 (d, 1H,  $J=8.3$  Hz), 6.48 (s, 1H), 2.70 (t, 2H,  $J=7.6$  Hz), 1.69–1.60 (m, 2H), 1.41–1.18 (m, 14H), 0.87 (t, 3H,  $J=6.2$ )  $\delta_C$  (100 MHz,  $CDCl_3$ ) 134.42, 134.4, 128.1, 124.1, 123.1, 119.8, 110.6, 102.3, 36.1, 32.3, 31.9, 29.7, 29.6, 29.4, 29.3, 22.7, 14.1.

**4.7.10. 5-Undecyl-1H-indole (5j).** Pale yellow solid. 55% yield. Mp: 53–54 °C.  $\delta_H$  (400 MHz,  $CDCl_3$ ) 8.02 (br s, 1H), 7.43 (s, 1H), 7.29 (d, 1H,  $J=8.3$  Hz), 7.16 (t, 1H,  $J=2.6$  Hz), 7.03 (d, 1H,  $J=8.3$  Hz), 6.48 (s, 1H), 2.69 (t, 2H,  $J=7.6$  Hz), 1.69–1.60 (m, 2H), 1.41–1.18 (m, 16H), 0.87 (t, 3H,  $J=6.4$ )  $\delta_C$  (100 MHz,  $CDCl_3$ ) 134.4, 134.3, 128.1, 124.1, 123.1, 119.8, 110.6, 102.3, 36.1, 32.3, 31.9, 29.7, 29.63, 29.6, 29.4, 29.3, 22.7, 14.1.

**4.7.11. 5-Dodecyl-1H-indole (5k).** Pale yellow solid. 72% yield. Mp: 48–50 °C.  $\delta_H$  (400 MHz,  $CDCl_3$ ) 8.03 (br s, 1H), 7.43 (s, 1H), 7.29 (d, 1H,  $J=8.3$  Hz), 7.16 (t, 1H,  $J=2.6$  Hz), 7.03 (d, 1H,  $J=8.3$  Hz), 6.48 (s, 1H), 2.69 (t, 2H,  $J=7.6$  Hz), 1.69–1.60 (m, 2H), 1.41–1.17 (m, 18H), 0.88 (t, 3H,  $J=6.4$ )  $\delta_C$  (100 MHz,  $CDCl_3$ ) 134.4, 134.3, 128.1, 124.1, 123.1, 119.8, 110.6, 102.3, 36.1, 32.3, 31.9, 29.7, 29.63, 29.6, 29.4, 29.3, 22.7, 14.1.

**4.7.12. 5-Tridecyl-1H-indole (5l).** Pale yellow solid. 57% yield. Mp: 63–64 °C.  $\delta_H$  (400 MHz,  $CDCl_3$ ) 8.03 (br s, 1H), 7.43 (s, 1H), 7.30 (d, 1H,  $J=8.3$  Hz), 7.17 (t, 1H,  $J=2.5$  Hz), 7.03 (d, 1H,  $J=8.3$  Hz), 6.49 (s, 1H), 2.69 (t, 2H,  $J=7.6$  Hz), 1.69–1.60 (m, 2H), 1.41–1.17 (m, 20H),

0.88 (t, 3H,  $J=6.5$ )  $\delta_C$  (100 MHz,  $CDCl_3$ ) 134.4, 134.3, 128.1, 124.1, 123.1, 119.8, 110.6, 102.3, 36.1, 32.33, 32.3, 31.9, 29.7, 29.66, 29.62, 29.42, 29.4, 29.3, 22.3, 14.14, 14.1.

**4.7.13. 5,5'-Dimethyl indigo (C1).** A mixture of 5-methylindole **5m** (165 mg, 1.26 mmol), tBuOH (500 mg), Cumene hydroperoxide (80% grade, 120 mg), acetic acid (2 mg), and  $Mo(CO)_6$  (0.2 mg) was heated to reflux for 30 min. During reaction at reflux temperature, the pale yellow reaction mixture of color was changed to red-green, dark red, then precipitated blue solids. After cooling, the suspended reaction mixture was filtered and successively washed with EtOH, hexane, and  $CH_2Cl_2$ . Blue solid was obtained in 57% yield (103 mg, 0.36 mmol), mp: >300 °C. UV/Vis:  $\lambda_{max}$  (1,2-DCB), 615 nm (log $\epsilon$ , 4.23).  $\delta_H$  (600 MHz,  $CDCl_3$ ) 8.80 (s, 2H,  $J=8.4$  Hz), 7.53 (s, 2H), 7.31 (d, 2H,  $J=8.4$  Hz), 6.94 (d, 2H,  $J=8.6$  Hz), 2.35 (s, 6H). HRMS (FAB,  $[M+H]^+$ ): calcd for  $C_{18}H_{15}N_2O_2$ : 291.1134, found 291.1169. IR (KBr):  $\nu(NH)$  3295  $cm^{-1}$ ,  $\nu(CH)$  3027, 2915, 2858  $cm^{-1}$ ,  $\nu(C=O)$  1633, 1620, 1587  $cm^{-1}$ .

Compound **C2–C13** were synthesized according to the similar procedure as that of **C1**.

**4.7.14. 5,5'-Diethyl indigo (C2).** Blue solid. 48% yield. Mp: >300 °C. UV/Vis:  $\lambda_{max}$  (1,2-DCB), 615 nm (log $\epsilon$ , 4.25).  $\delta_H$  (400 MHz,  $CDCl_3$ ) 8.82 (s, 2H), 7.56 (s, 2H), 7.34 (d, 2H,  $J=8.7$  Hz), 6.97 (d, 2H,  $J=8.1$  Hz), 2.65 (dd, 4H,  $J=14.5, 7.5$  Hz), 1.25 (t, 6H,  $J=7.5$  Hz). HRMS (FAB,  $[M]^+$ ): calcd for  $C_{20}H_{18}N_2O_2$ : 318.1368, found 318.1371. lit<sup>24</sup>. Mp: 373–374 °C (chlorobenzene), UV/Vis:  $\lambda_{max}$  610–612 nm (KBr, n.b.). IR (KBr):  $\nu(NH)$  3306  $cm^{-1}$ ,  $\nu(CH)$  3018, 2960, 2932, 2871  $cm^{-1}$ ,  $\nu(C=O)$  1634, 1620, 1588  $cm^{-1}$ .

**4.7.15. 5,5'-Dipropyl indigo (C3).** Blue solid. 33% yield. Mp: >300 °C. UV/Vis:  $\lambda_{max}$  (DCB), 615 nm (log $\epsilon$ , 4.27).  $\delta_H$  (400 MHz,  $CDCl_3$ ) 8.82 (s, 2H), 7.54 (s, 2H), 7.31 (dd, 2H,  $J=8.2, 1.4$  Hz), 6.96 (d, 2H,  $J=8.2$  Hz), 2.59 (t, 4H,  $J=7.4$  Hz), 1.71–1.58 (m, 4H), 0.94 (t, 6H,  $J=7.4$  Hz).  $\delta_C$  (100 MHz,  $CDCl_3$ ) 188.9, 150.4, 136.8, 135.4, 123.6, 121.9, 120.2, 111.9, 37.3, 24.6, 13.6. HRMS (FAB,  $[M]^+$ ): calcd for  $C_{22}H_{22}N_2O_2$ : 346.1681, found 346.1682.

IR (KBr):  $\nu(NH)$  3297  $cm^{-1}$ ,  $\nu(CH)$  3017, 2956, 2927, 2863  $cm^{-1}$ ,  $\nu(C=O)$  1632, 1618, 1588  $cm^{-1}$ .

**4.7.16. 5,5'-Dibutyl indigo (C4).** Blue solid. 31% yield. Mp: >300 °C. UV/Vis:  $\lambda_{max}$  (DCB), 616 nm (log $\epsilon$ , 4.28).  $\delta_H$  (400 MHz,  $CDCl_3$ ) 8.82 (s, 2H), 7.54 (s, 2H), 7.32 (dd, 2H,  $J=6.8, 1.5$  Hz), 6.96 (d, 2H,  $J=8.2$  Hz), 2.61 (t, 4H,  $J=7.5$  Hz), 1.67–1.55 (m, 4H), 1.40–1.31 (m, 4H), 0.93 (t, 6H,  $J=7.3$  Hz).  $\delta_C$  (100 MHz,  $CDCl_3$ ) 188.9, 150.3, 136.7, 135.6, 123.6, 121.9, 120.2, 111.9, 34.9, 33.7, 22.1, 13.9. HRMS (FAB,  $[M]^+$ ): calcd for  $C_{24}H_{26}N_2O_2$ : 374.1194, found 374.1193. lit<sup>24</sup>. Mp: 322–324 °C (benzene), UV/Vis:  $\lambda_{max}$  615 nm (benzene, 4.32). IR (KBr):  $\nu(NH)$  3372  $cm^{-1}$ ,  $\nu(CH)$  2955, 2926, 2868, 2853  $cm^{-1}$ ,  $\nu(C=O)$  1630, 1588  $cm^{-1}$ .

**4.7.17. 5,5'-Dipentyl indigo (C5).** Blue solid. 32% yield. Mp: >300 °C. UV/Vis:  $\lambda_{max}$  (DCB), 617 nm (log $\epsilon$ , 4.29).  $\delta_H$  (400 MHz,  $CDCl_3$ ) 8.82 (s, 2H), 7.54 (s, 2H), 7.32 (dd, 2H,  $J=6.8, 1.5$  Hz), 6.96 (d, 2H,  $J=8.2$  Hz), 2.60 (t, 4H,  $J=7.6$  Hz), 1.67–1.55 (m, 4H), 1.37–1.25 (m, 8H), 0.89 (t, 6H,  $J=6.8$  Hz).  $\delta_C$  (100 MHz,  $CDCl_3$ ) 188.9, 150.3, 136.7, 135.7, 123.6, 121.9, 120.2, 111.9, 35.2, 31.3, 31.2, 22.5, 14.0. HRMS (FAB,  $[M]^+$ ): calcd for  $C_{26}H_{30}N_2O_2$ : 402.2307, found 402.2305. lit<sup>24</sup>. Mp: 314 °C (benzene), UV/Vis:  $\lambda_{max}$  619 nm ( $CHCl_3$ , 4.28) IR (KBr):  $\nu(NH)$  3370  $cm^{-1}$ ,  $\nu(CH)$  2956, 2924, 2864, 2854  $cm^{-1}$ ,  $\nu(C=O)$  1630, 1616, 1587  $cm^{-1}$ .

**4.7.18. 5,5'-Dihexyl indigo (C6).** Blue solid. 42% yield. Mp: >300 °C. UV/Vis:  $\lambda_{max}$  (DCB), 617 nm (log $\epsilon$ , 4.30).  $\delta_H$  (400 MHz,  $CDCl_3$ )  $\delta_H$  (400 MHz,  $CDCl_3$ ) 8.82 (s, 2H), 7.54 (s, 2H), 7.31 (d, 2H,  $J=8.8$  Hz), 6.96 (d, 2H,  $J=8.6$  Hz), 2.60 (t, 4H,  $J=8.1$  Hz), 1.67–1.55 (m, 4H),

1.36–1.25 (m, 12H), 0.88 (t, 6H,  $J=6.5$  Hz). HRMS (FAB,  $[M]^+$ ): calcd for  $C_{28}H_{34}N_2O_2$ : 430.2620, found 430.2602. IR (KBr):  $\nu(NH)$  3371  $cm^{-1}$ ,  $\nu(CH)$  2953, 2919, 2848  $cm^{-1}$ ,  $\nu(C=O)$  1638, 1584  $cm^{-1}$ .

4.7.19. *5,5'-Diheptyl indigo (C7)*. Blue solid. 41% yield. Mp:  $>300$  °C. UV/Vis:  $\lambda_{max}$  (DCB), 617 nm ( $\log\epsilon$ , 4.27).  $\delta_H$  (400 MHz,  $CDCl_3$ )  $\delta_H$  (400 MHz,  $CDCl_3$ ) 8.82 (s, 2H), 7.54 (s, 2H), 7.31 (d, 2H,  $J=8.0$  Hz), 6.96 (d, 2H,  $J=8.1$  Hz), 2.60 (t, 4H,  $J=7.9$  Hz), 1.67–1.55 (m, 4H), 1.35–1.24 (m, 16H), 0.88 (t, 6H,  $J=6.9$  Hz). HRMS (FAB,  $[M]^+$ ): calcd for  $C_{30}H_{38}N_2O_2$ : 458.2933, found 458.2934. IR (KBr):  $\nu(NH)$  3375  $cm^{-1}$ ,  $\nu(CH)$  2955, 2924, 2869, 2854  $cm^{-1}$ ,  $\nu(C=O)$  1628, 1584  $cm^{-1}$ .

4.7.20. *5,5'-Dioctyl indigo (C8)*. Blue solid. 42% yield. Mp:  $>300$  °C. UV/Vis:  $\lambda_{max}$  (DCB), 617 nm ( $\log\epsilon$ , 4.26).  $\delta_H$  (400 MHz,  $CDCl_3$ )  $\delta_H$  (400 MHz,  $CDCl_3$ ) 8.81 (s, 2H), 7.54 (s, 2H), 7.31 (d, 2H,  $J=9.5$  Hz), 6.96 (d, 2H,  $J=8.2$  Hz), 2.60 (t, 4H,  $J=7.4$  Hz), 1.67–1.55 (m, 4H), 1.35–1.24 (m, 20H), 0.88 (t, 6H,  $J=6.4$  Hz). HRMS (FAB,  $[M]^+$ ): calcd for  $C_{32}H_{42}N_2O_2$ : 486.3246, found 486.3244. lit<sup>24</sup>. Mp: 284–285 °C (benzene), UV/Vis:  $\lambda_{max}$  605 nm (KBr, n.b.) IR (KBr):  $\nu(NH)$  3375  $cm^{-1}$ ,  $\nu(CH)$  2954, 2924, 2850  $cm^{-1}$ ,  $\nu(C=O)$  1630, 1614, 1586  $cm^{-1}$ .

4.7.21. *5,5'-Dinonyl indigo (C9)*. Blue solid. 37% yield. Mp: 298–299 °C. UV/Vis:  $\lambda_{max}$  (DCB), 617 nm ( $\log\epsilon$ , 4.26).  $\delta_H$  (400 MHz,  $CDCl_3$ )  $\delta_H$  (400 MHz,  $CDCl_3$ ) 8.81 (s, 2H), 7.54 (s, 2H), 7.31 (d, 2H,  $J=8.2$  Hz), 6.96 (d, 2H,  $J=9.3$  Hz), 2.60 (t, 4H,  $J=7.5$  Hz), 1.65–1.55 (m, 4H), 1.36–1.20 (m, 24H), 0.88 (t, 6H,  $J=6.6$  Hz). HRMS (FAB,  $[M]^+$ ): calcd for  $C_{34}H_{46}N_2O_2$ : 514.3599 found 514.3525. IR (KBr):  $\nu(NH)$  3375  $cm^{-1}$ ,  $\nu(CH)$  2956, 2924, 2852  $cm^{-1}$ ,  $\nu(C=O)$  1631, 1613, 1585  $cm^{-1}$ .

4.7.22. *5,5'-Didecyl indigo (C10)*. Blue solid. 42% yield. Mp: 288–289 °C. UV/Vis:  $\lambda_{max}$  (DCB), 617 nm ( $\log\epsilon$ , 4.27).  $\delta_H$  (400 MHz,  $CDCl_3$ ) 8.83 (s, 2H), 7.54 (s, 2H), 7.31 (d, 2H,  $J=8.1$  Hz), 6.96 (d, 2H,  $J=8.2$  Hz), 2.60 (t, 4H,  $J=7.3$  Hz), 1.77–1.57 (m, 4H), 1.35–1.24 (m, 28H), 0.88 (t, 6H,  $J=6.6$  Hz). HRMS (FAB,  $[M]^+$ ): calcd for  $C_{36}H_{50}N_2O_2$ : 542.3872 found 542.3871. IR (KBr):  $\nu(NH)$  3378  $cm^{-1}$ ,  $\nu(CH)$  2956, 2917, 2847  $cm^{-1}$ ,  $\nu(C=O)$  1631, 1613, 1587  $cm^{-1}$ .

4.7.23. *5,5'-Diundecyl indigo (C11)*. Blue solid. 39% yield. Mp: 285–286 °C. UV/Vis:  $\lambda_{max}$  (DCB), 617 nm ( $\log\epsilon$ , 4.26).  $\delta_H$  (400 MHz,  $CDCl_3$ ) 8.81 (s, 2H), 7.54 (s, 2H), 7.31 (d, 2H,  $J=8.6$  Hz), 6.96 (d, 2H,  $J=8.2$  Hz), 2.60 (t, 4H,  $J=7.4$  Hz), 1.65–1.56 (m, 4H), 1.37–1.20 (m, 32H), 0.88 (t, 6H,  $J=6.3$  Hz). HRMS (FAB,  $[M]^+$ ): calcd for  $C_{38}H_{54}N_2O_2$ : 570.4185 found 570.4187. IR (KBr):  $\nu(NH)$  3382  $cm^{-1}$ ,  $\nu(CH)$  2956, 2917, 2848  $cm^{-1}$ ,  $\nu(C=O)$  1630, 1612, 1585  $cm^{-1}$ .

4.7.24. *5,5'-Didodecyl indigo (C12)*. Blue solid. 40% yield. UV/Vis:  $\lambda_{max}$  (DCB), 617 nm ( $\log\epsilon$ , 4.27). Mp: 274–275 °C  $\delta_H$  (400 MHz,  $CDCl_3$ ) 8.83 (s, 2H), 7.54 (s, 2H), 7.31 (d, 2H,  $J=8.9$ , 2.2 Hz), 6.96 (d, 2H,  $J=8.0$  Hz), 2.60 (t, 4H,  $J=7.8$  Hz), 1.68–1.49 (m, 4H), 1.35–1.24 (m, 36H), 0.88 (t, 6H,  $J=6.7$  Hz). HRMS (FAB,  $[M]^+$ ): calcd for  $C_{40}H_{58}N_2O_2$ : 598.4498 found 598.4499. IR (KBr):  $\nu(NH)$  3380  $cm^{-1}$ ,  $\nu(CH)$  2956, 2917, 2848  $cm^{-1}$ ,  $\nu(C=O)$  1630, 1614, 1589  $cm^{-1}$ .

4.7.25. *5,5'-Ditridecyl indigo (C13)*. Blue solid. 39% yield. Mp: 264, 265 °C. UV/Vis:  $\lambda_{max}$  (DCB), 617 nm ( $\log\epsilon$ , 4.26).  $\delta_H$  (600 MHz,  $CDCl_3$ ) 8.83 (s, 2H), 7.56 (s, 2H), 7.34 (d, 2H,  $J=9.5$  Hz), 6.98 (d, 2H,  $J=8.2$  Hz), 2.62 (t, 4H,  $J=8.0$  Hz), 1.67–1.57 (m, 4H), 1.38–1.22 (m, 40H), 0.90 (t, 6H,  $J=6.8$  Hz). HRMS (FAB,  $[M]^+$ ): calcd for

$C_{42}H_{62}N_2O_2$ : 626.4811 found 626.4820. IR (KBr):  $\nu(NH)$  3380  $cm^{-1}$ ,  $\nu(CH)$  2955, 2917, 2846  $cm^{-1}$ ,  $\nu(C=O)$  1629, 1612, 1585  $cm^{-1}$ .

## Acknowledgements

This work was supported by a Grant-in-Aid for Science Research (YB 26810107) from the Ministry of Education, Culture, Sports, Science and Technology (MEXT), Japan, and was performed under the Cooperative Research Program of “Network Joint Research Centre for Materials and Devices (IMCE, Kyushu University)”. MW acknowledge support from I<sup>2</sup>CNER, funded by the World Premier International Research Centre Initiative (WPI), Ministry of Education, Culture, Sports, Science and Technology of Japan (MEXT), Japan. The computations were carried out by using the computer facilities at the Research Institute for Information Technology, Kyushu University.

## Supplementary data

Supplementary data related to this article can be found at <http://dx.doi.org/10.1016/j.tet.2016.05.069>.

## References and notes

- Kettner, F.; Hüter, L.; Schäfer, J.; Röder, K.; Purgahn, U.; Krautscheid, H. *Acta Cryst. Sec. E* **2011**, *67*, o2867.
- Kojima, H.; Mori, T. *Chem. Lett.* **2013**, *42*, 68.
- Moreno, M.; Ortiz-Sánchez, J. M.; Gelabert, R.; Lluch, J. M. *Phys. Chem. Chem. Phys.* **2013**, *15*, 20236.
- Amat, A.; Rosi, F.; Miliani, C.; Sgamellotti, A.; Fantacci, S. *J. Mol. Struct.* **2011**, *993*, 43.
- Głowacki, E. D.; Voss, G.; Sariciftci, N. S. *Adv. Mater.* **2013**, *25*, 6783.
- Głowacki, E. D.; Voss, G.; Leonat, L.; Irimia-Vladu, M.; Bauer, Sariciftci, N. S. *Isr. J. Chem.* **2012**, *52*, 1.
- Irimia-Vladu, M.; Głowacki, E. D.; Troshin, P. A.; Schwabegger, G.; Leonat, L.; Susarova, D. K.; Krystal, O.; Ullah, M.; Kanbur, Y.; Bodea, M. A.; Razumov, V. F.; Sitter, H.; Bauer, Sariciftci, N. S. *Adv. Mater.* **2012**, *24*, 375.
- Joby, N. G.; Venkatachalam, P.; Krishnakumar, N. *Int. J. Sci. Eng. Res.* **2013**, *4*, 1317.
- Abdullah, M. I.; Janjua, M. R. S. A.; Mahmood, A.; Ali, S.; Ali, M. *Bull. Korean Chem. Soc.* **2013**, *34*, 2093.
- Alexy, M.; Voss, G.; Heinze, J. *Anal. Bioanal. Chem.* **2005**, *382*, 1628.
- Brunet, J.; Spinelle, L.; Ndiaye, A.; Dubois, M.; Monier, G.; Varenne, C.; Pauly, A.; Lauron, B.; Guerin, K.; Hamwi, A. *Thin Solid Films* **2011**, *520*, 971.
- Yao, M.; Araki, M.; Senoh, H.; Yamazaki, S.; Sakai, T.; Yasuda, K. *Chem. Lett.* **2010**, *39*, 950.
- Yao, M.; Kuratani, K.; Kojima, T.; Takeichi, N.; Senoh, H.; Kiyobayashi, T. *Sci. Rep.* **2014**, *4*, 3650.
- Pitayatanakul, O.; Higashino, T.; Kadoya, T.; Tanaka, M.; Kojima, H.; Ashizawa, M.; Kawamoto, T.; Matsumoto, H.; Ishikawa, K.; Mori, T. *J. Mater. Chem. C* **2014**, *2*, 9311.
- Pitayatanakul, O.; Higashino, T.; Kadoya, T.; Tanaka, M.; Kojima, H.; Ashizawa, M.; Kawamoto, T.; Matsumoto, H.; Ishikawa, K.; Mori, T. *J. Mater. Chem. C* **2015**, *3*, 8612.
- Klimovich, I. V.; Leshanskaya, L. I.; Troyanov, S. I.; Anokhin, D. V.; Novikov, D. V.; Piryazev, A. A.; Ivanov, D. A.; Dremova, N. N.; Troshin, P. A. *J. Mater. Chem. C* **2014**, *2*, 7621.
- Miskiewicz, P.; Mas-Torrent, M.; Jung, J.; Kotarba, S.; Głowacki, I.; Gomar-Nadal, E.; Amabilino, D. B.; Veciana, J.; Krause, B.; Carbone, D.; Rovira, C.; Ulanski, J. *Chem. Mater.* **2006**, *18*, 4724.
- Generali, G.; Dinelli, F.; Capelli, R.; Toffanin, S.; di Maria, F.; Gazzano, M.; Barbarella, G.; Muccini, M. *J. Phys. Chem. C* **2011**, *115*, 23164.
- An, T. K.; Jang, S. H.; Kim, S.-O.; Jang, J.; Hwang, J.; Cha, H.; Noh, Y. R.; Yoon, S. B.; Yoon, Y. J.; Kim, L. H.; Chung, D. S.; Kwon, S.-K.; Kim, Y.-H.; Lee, S.-G.; Park, C. E. *Chem.—Eur. J.* **2013**, *19*, 14052.
- Back, J. Y.; An, T. K.; Cheon, Y. R.; Cha, H.; Jang, J.; Kim, Y.; Baek, Y.; Chung, D. S.; Kwon, S.-K.; Park, C. E.; Kim, Y.-H. *ACS Appl. Mater. Interfaces* **2015**, *7*, 351.
- Takimiya, K.; Shinamura, S.; Osaka, I.; Miyazaki, E. *Adv. Mater.* **2011**, *23*, 4347.
- Zhang, F.; Hu, Y.; Schuettfort, T.; Di, C.; Gao, X.; McNeill, C. R.; Thomsen, L.; Mannsfeld, S. C. B.; Yuan, W.; Sirringhaus, H.; Zhu, D. *J. Am. Chem. Soc.* **2013**, *135*, 2338.
- Lei, T.; Wang, J.-Y.; Pei, P. *Chem. Mater.* **2014**, *26*, 594.
- Meier, H.; Lütte, W. *Liebigs Ann. Chem.* **1981**, 1303.
- Yamamoto, Y.; Inoue, Y.; Takaki, U.; Suzuki, H. *Bull. Chem. Soc. Jpn.* **2011**, *84*, 82.
- Buscio, V.; Crespi, M.; Gutiérrez-Bouzán, C. *Materials* **2014**, *7*, 6184.